New Advances in Space SHM Project

Adrian TOADER[1], Ioan URSU*,[1], Daniela ENCIU[1]

*Corresponding author
*,[1]INCAS – National Institute for Aerospace Research "Elie Carafoli"
B-dul Iuliu Maniu 220, Bucharest 061126, Romania
toader.adrian@incas.ro, ursu.ioan@incas.ro*, enciu.daniela@incas.ro

DOI: 10.13111/2066-8201.2015.7.1.7

Abstract: *This paper is based on a consistent family of experimental data obtained in a national research project. More accurate, specimens representing spacecraft structures, accomplished from aluminum circular plates with PWAS bonded on them were subjected to extreme temperature variations and radiations, both specific to space applications. The structure itself is affected by mechanical damages caused by fatigue and aging. These mechanical damages were simulated by laser fabricated slit cuts. The signature of structure's health is seen as the real part of electromechanical impedance (EMI) curves of a PWAS bonded on structure. Whatever the EMI signature (recorded via special devices) changes, it is important that it be signaled online. It is shown that a neural network (NN) has the willingness to "learn", thus identifying a function more or less complicated, as it is the case with the real part of EMI characteristic. In view of NN preparation for in-situ installing, at least the following aspects must be elucidated: setting the number of iterations to learning; evaluation of common damages that can appear in the structure; investigations on their evolution time; investigations on the possible values of learning errors; the default value of error to stop the learning process.*

Key Words: *spacecraft structures, structural health monitoring, piezoelectric wafer active sensors, electromechanical impedance, online identification, neural networks.*

1. INTRODUCTION

A quick foray into technical literature reveales that only very few references are dedicated to Space applications of SHM technologies (e.g., [1], [2], [3], [4]), even if the Space Shuttle Challenger disaster (January 28, 1986) [5] and, some time ago, Columbia Space Shuttle disaster (February 1, 2003) (see [6] and Fig. 1) have raised several questions about the possible, just required, use of sensors for in-space SHM. So, after the Columbia Accident Investigation Board issued its Report [6] in August 2003, NASA decided to add sensors to the Space Shuttle to detect any blows from debris and to produce alerts if leading edges of the wings were hit. However, these sensors were not sufficiently advanced to determine the degree of damage, and the extent of damage would still have to be determined by an inspection by astronauts in orbit using an extension boom equipped with cameras and lasers. A natural question might be "assuming that a vehicle health management system could have been in operation, could the Columbia mission have been saved?" [7]. Of course, the question is rhetorical. As can see from the few materials available, space SHM technology is very recent [3]. These issues still persist, but the integration of SHM technology into space vehicles design process still faces skepticism.

However, it is expected that the interest in space SHM technologies will grow in direct proportion to the interest on reusable space vehicles in state-sponsored, commercial, or private-public space enterprises. Thus, it is estimated (meetings of the SAE Aerospace

Industry Steering Committee on SHM, http://www.sae.org/standardsdev/news/P91616.pdf) that the use of SHM technologies in the aircraft and ground vehicle may increase ten-fold in the coming decades.)

The development of real-time SHM techniques involves among others the design of an in-situ damage detection methodology and also the off-line study of the damage severity based on the evaluation of damage metrics [8]).

The present paper is backed by a database consisting on a large amount of experimental data obtained in the STAR project code ID 188/2012 "Structural health monitoring in spacecraft structures using piezoelectric wafer active sensors (PWAS) multimodal guided waves", supported by National Authority for Scientific Research−ANCS, UEFISCSU [4], [9], [10]. The experimental part of the project addresses a problem specific to space applications, namely the effect on the PWAS EMI method of the extreme temperature variations and space radiations. Some aspects of these tests are given in Section 2.

The problem selected to be widely exposed in article is that of "online identification of faults", and is based on the property of universal approximator of a neural network (NN). In other words, theoretically speaking, a (NN) can be trained "to learn" the current shape of the graph, defined over a set of frequencies, which represents (electromechanical impedance) EMI recording of a healthy structure. The occurrence of a fault would mean changing the graph, and will be ratified by the occurrence of an error, which is the difference between healthy structure and "the sick" structure. Therefore, imagine the following scenario. Suppose that there is an on-line impedance analyzer, which provides the EMI shape of healthy structure; the same device will catch the moment when the structure becomes damaged. In parallel with this hard system, there is a software package based on NNs, which will indicate and quantify the occurrence of a problem. Theoretical problem is formulated and solved on a case by case basis depending on the physical problem. The latter will take into account the given structure and the type of common faults (cracks, delaminations, typical damage of PZT material, of adhesive etc.; in fact, many electronics failures are really mechanical failures). Ultimately, to establish criteria for monitoring the NN structure will count the rate of evolution of these faults [11].

2. TESTS, RECORDS AND DATA PROCESSING IN THE PROJECT "SPACE SHM"

A considerable amount of testing stages, EMI records, data processing and analytical assessments on damage identification, in order to qualify PWAS transducers, and, more generally, SHM methodology, for use in space operations were performed in INCAS "Elie Carafoli" (see www.incas.ro) and IFIN-HH (see www.nipne.ro) labs in the years 2013, 2014. The records refer to either PWASs or specimens with bonded PWAS, without and with simulated defects. PWAS purchased from the company STEMINC (http://www.steminc.com/) were glued with glue M-Bond 610 Vishay [12] on the aluminum circular plate of 100 mm diameter and 0.2 mm thick. Mechanical damages were simulated as laser fabricated narrow through-the-thickness slit cuts (Fig. 1).

The following conditions, simulating space conditions, were provided at IFIN-HH lab: a) absorbed doses: 100 Gy ... 20 kGy (1Gy = 1J/1kg); b) dose rate: 20Gy/h ... 100Gy/h; c) vacuum pressure $<10^{-1}$Pa; d) extreme temperatures: between -150^0C (77K) and $+175^0$C.

The definition of extreme temperature cycles: from -196^0C (77K, liquid nitrogen temperature) to $+150^0$C (the temperature for which the tests were carried out at INCAS in 2013); number of cycles: minimum 10 (low temperature → back to room temperature → high

temperature); cycle length: ~ 10h, each area of extreme temperature and 2 hours for recovery and storage at room temperature. Thus a complete cycle was performed in 24 hours.

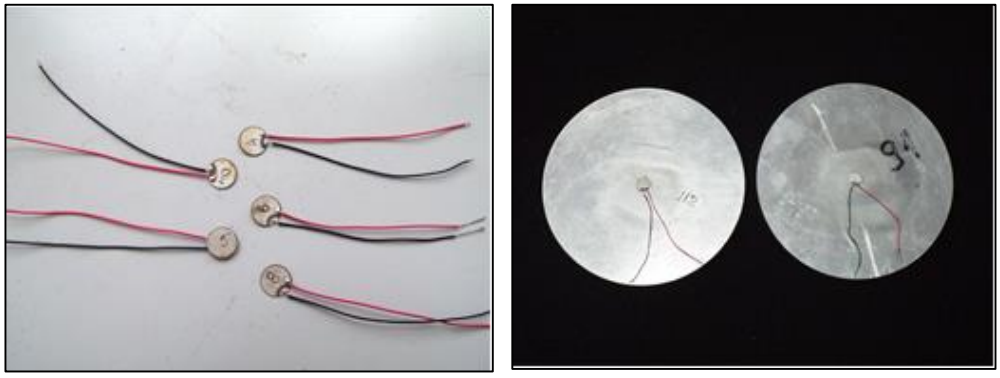

Fig. 1 – STEMINC PWASs # 4, 5. 6. 8, 9 and circular specimens S91, S 118, with central bonded PWAS, with and, respectively, without simulated mechanical damage

Extreme temperature and radiations were applied simultaneously at IFIN-HH to the pristine and "damaged" samples. EMI signatures were raised, as appropriate, on line (i.e., during the submission of proof at harsh conditions), or offline (after submission, i.e. at room temperature and without radiation), see an example in Fig. 2. It is to emphasize that getting a consistent database for statistical interpretation of the results was envisaged during the project implementation.

Based on these EMI records, damage metrics were calculated as root mean square deviation (RMSD) [13], [8] from healthy to damaged specimen (see Tables 1-3). Since the EMI signature does not always clarify the origin of the defects – mechanical or electronic, generated by fatigue and the aging of the structure, or by deficiencies of sensors bonding on the specimen etc. – , special investigative means were added. For example, during testing in harsh conditions (of temperature and irradiation), reversible changes in EMI signatures can occur, in the sense that these changes will disappear when the conditions will disappear. These changes should somehow be monitored, and a damage indicator (DI) should be recalculated based on some compensation techniques [14] in order to not trigger false alarms. Such compensation techniques have also been used in the project, see the representative values given in Fig. 3, assessed on the basis of two different methods.

Other putative causes of EMI signature changes were a) unfulfilment of an adequate bonding of PWAS to the specimen, and b) damage of PWAS itself. To this end, a research travel was done at Laboratory for Active Materials and Smart Structures (LAMSS), University of South Carolina, which resulted in a large volume of measurements and recordings of microscopy and vibration applied to a number of PWASs and disk specimens. A state of the art specialized equipment for performing active materials and smart structures research was used. First of all, *Polytec PSV-400 Scanning Vibrometer* (Fig. 4, left) for non-contact measurement, visualization and analysis of structural vibrations. This is a measurement tool for non-contact measurement, visualization and analysis of structural vibrations. It determines the operational deflection shapes and eigen modes as easily as taking a photograph. Entire surfaces can be scanned and probed automatically using flexible and interactive measurement grids. Measurements can be made over a wide frequency bandwidth.

Designed for resolving noise and vibration issues in R&D and manufacturing, the system is versatile and easy to use. At the heart of every Polytec PSV-400 system is the laser-Doppler vibrometer – a precision optical transducer used for determining vibration velocity and

displacement at a fixed point. The technology is based on the Doppler-effect; sensing the frequency shift of back scattered light from a moving surface. More details of this technology on: www.polytec.com/vib-universit.

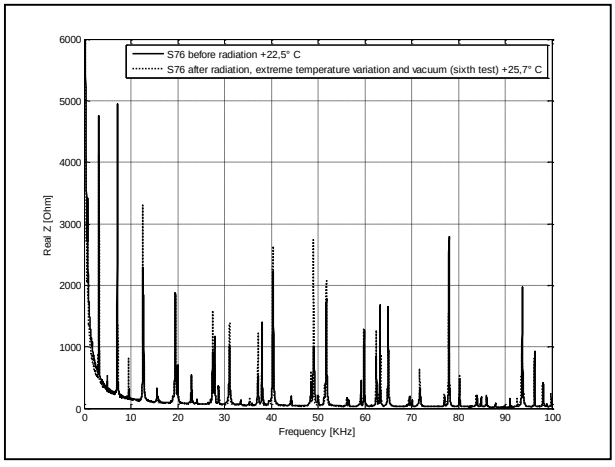

Fig. 2 – EMI signature for specimen disk # 76 with defect of arc type, before and after subjecting to radiations and extreme temperatures cycling

Table 1 – room temperature

type of specimen	metrics	
	RMSD	CC
pristine vs. arc 7	0.919	0.496
pristine vs. arc 15	0.822	0.548
pristine vs. arc 25	0.895	0.567
pristine vs. arc 45	0.749	0.564
pristine vs. line 25	1.484	0.243
pristine vs. line 45	0.964	0.505

Table 2 – high temperature (150° C)

type of specimen	metrics	
	RMSD	CC
pristine vs. arc 7	0.874	0.548
pristine vs. arc 15	0.805	0.576
pristine vs. arc 25	1.116	0.502
pristine vs. arc 45	0.818	0.515
pristine vs. line 25	1.349	0.281
pristine vs. line 45	0.915	0.570

Table 3 – room temperature (after 150° C)

type of specimen	metrics	
	RMSD	CC
pristine vs. arc 7	0.868	0.581
pristine vs. arc 15	0.547	0.749
pristine vs. arc 25	0.627	0.709
pristine vs. arc 45	0.552	0.749
pristine vs. line 25	1.162	0.419
pristine vs. line 45	0.741	0.694

# PZT	RMSD before compensation	RMSD after compensation
200	0.4308	0.2097
201	0.4026	0.2523
203	0.1889	0.1447
204	0.1586	0.1584
209	0.2778	0.2082
210	0.2825	0.2005
215	0.4781	0.2090
218	0.2332	0.2246
2220	0.2921	0.2816

Fig. 3 – Some results on the RMSD size induced as reversible effects of harsh conditions

Fig. 4 – LAMSS, UofSC equipment used in the project; left: Scanning Laser Doppler Vibrometer (SLDV; Polytec PSV-400); middle: SAM 300 scanning acoustic microscope (http://www.pva-analyticalsystems.com); right: digital microscope VHX 5000 **(**www.keyence.co.uk/)

Fig. 5 shows one of the multiple recordings done in *time domain* with SLDV. The specimen disk # 138 (with arc type defect at 15 mm) is scanned at a frequency of **2738 Hz**, see a 3D representation. One can see the position of the defect as red peak. Next to the picture is the color scale. The red bar indicates when the image is selected: at 0.0723 ms. The displacement is given in [nm], depending on time [ms] (vibration measured in the z-direction, perpendicular to the disk, takes also negative values). The graph refers to a vibration of a specific point on the surface of the disk otherwise indicated in the picture.

Fig. 6 shows the use of SLDV for records in the frequency domain. For the same specimen # 138, a 3D image of the vibration at a frequency of 49.56 kHz is shown. The displacement graph is associated to a certain point on the disk, and indicates the vibration of this point depending on the frequency.

Of course, EMI signatures were made at LAMSS, but these are current also at INCAS, Mechatronics Lab, by using the HP 4194 impedance analyzer.

Another tool used was the *SAM 300 scanning acoustic microscope*. This is mainly dedicated to high throughput, non-destructive analysis for quality control and research applications. The system enables detailed acoustic investigations through new radio frequency and transducer technologies of up to 400 MHz. Built to industry standards around a core platform that utilizes the latest production and research technology, the SAM 300 series has an ultrasound frequency range up to 500 MHz with transducers in the range 5 MHz – 400 MHz. Scanning range: x=250 µm-320 mm, y=250 µm-320 mm, z=100mm.

Fig. 7 shows images obtained with this device, at investigating the disk #122, particularly chosen wrong, for study. One can see: cracks in PZT (red circles); a piece of PZT is broken (green rectangle); areas without glue (yellow rhombs).

Finally, a third device used was the *digital microscope VHX 5000*. The VHX is an all-in-one microscope that incorporates observation, image capture, and measurement capabilities. Fig.8 shows two images of the disk # 106 obtained with this device. The picture on the right is an enlarged image of the left side; a crack is shown in PZT.

3. ONLINE IDENTIFICATION OF DAMAGES

The original formalism of artificial neural networks (ANN, in short, NN) derived from modeling of cognitive processes. Any NN must have two characteristics: a) to contain a learning algorithm, based on tuning sets of adaptive weights and b) to be capable of

approximating nonlinear functions [15], [16]. Both properties are exploited in the proposed method online identification of defects.

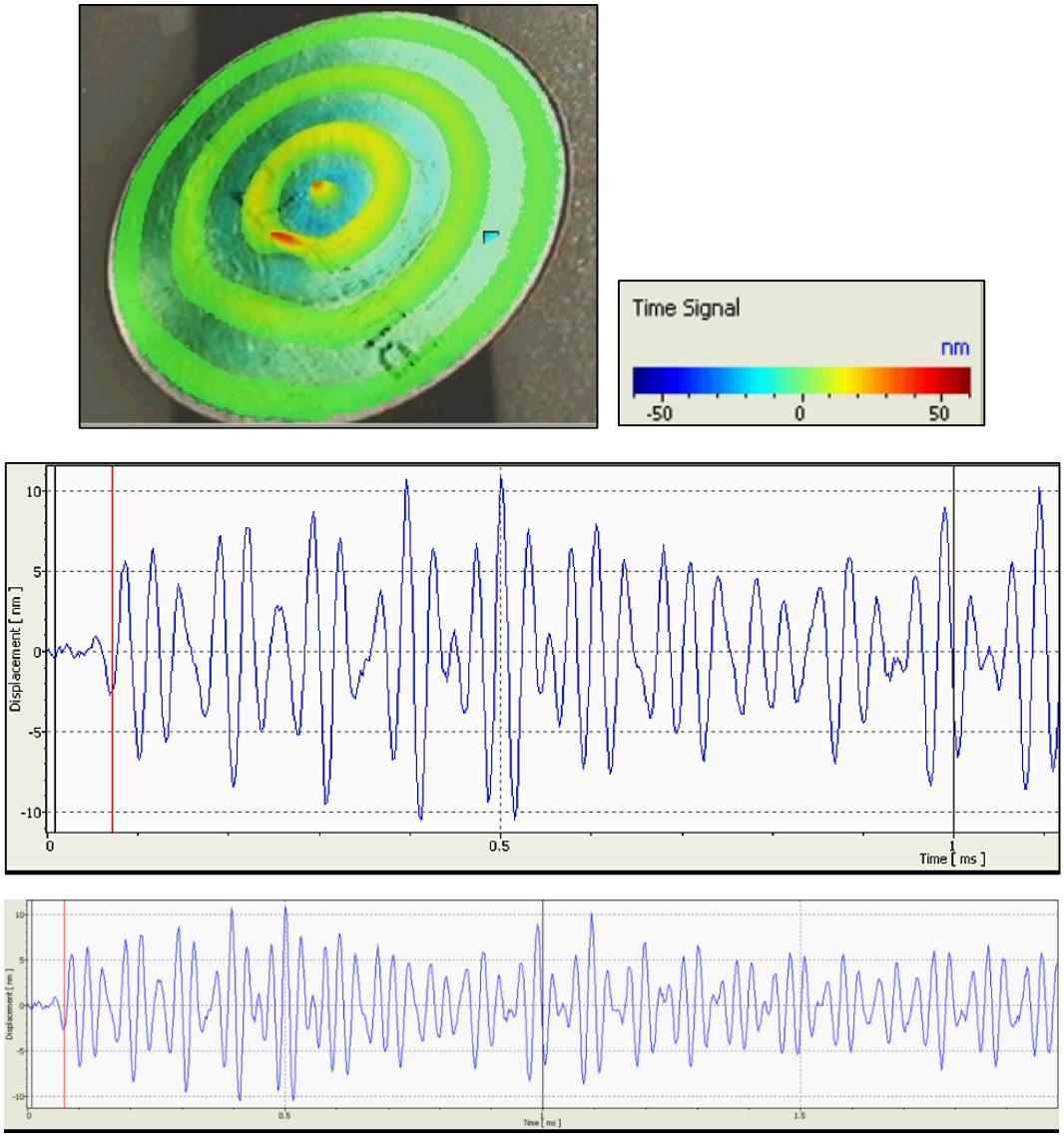

Fig. 5 – Recordings in time domain done with SLDV on specimen disk #138 (the registration below indicates a certain stabilization of vibration)

For better understanding of the ideas let's remember some words about the second property. In the mathematical theory of NN, the universal approximation theorem states that a feed-forward network with a single hidden layer containing a finite number of neurons (i.e., a multilayer perceptron), can approximate continuous functions on compact subsets of R^n, under assumptions on the activation function (non-constant, bounded, and monotonically-increasing continuous function, the so called sigmoid function; e. g., $f(x) = \left(1 + e^{-x}\right)^{-1}$). One of the first versions of the theorem is given for sigmoid activation functions [17].

NNs often have multilayer structures. For instance, the sigmoid model

$$u_i = \sum_{j=1}^{N} a_{ij}\sigma\left(\boldsymbol{b}_{ij}^{\mathrm{T}}\boldsymbol{Y} + d_{ij}\right), i = 1,2,\ldots,q \tag{1}$$

with $a_{ij}, d_{ij} \in R, \boldsymbol{b}_{ij} \in \mathrm{R}^{mp+qn}$, has an input layer, a sigmoid hidden layer, and a linear output layer. Kolmogorov theorem [18] shows that any continuous function in the *n*-dimensional cube E^n $(E = [0,1])$ can be represented as

$$f(x_1,\ldots,x_n) = \sum_{i=1}^{2n+1}\chi_i\left(\sum_{j=1}^{n}\phi_{ij}(x_j)\right) \tag{2}$$

where χ_i and ϕ_{ij} are continuous real functions of one variable.

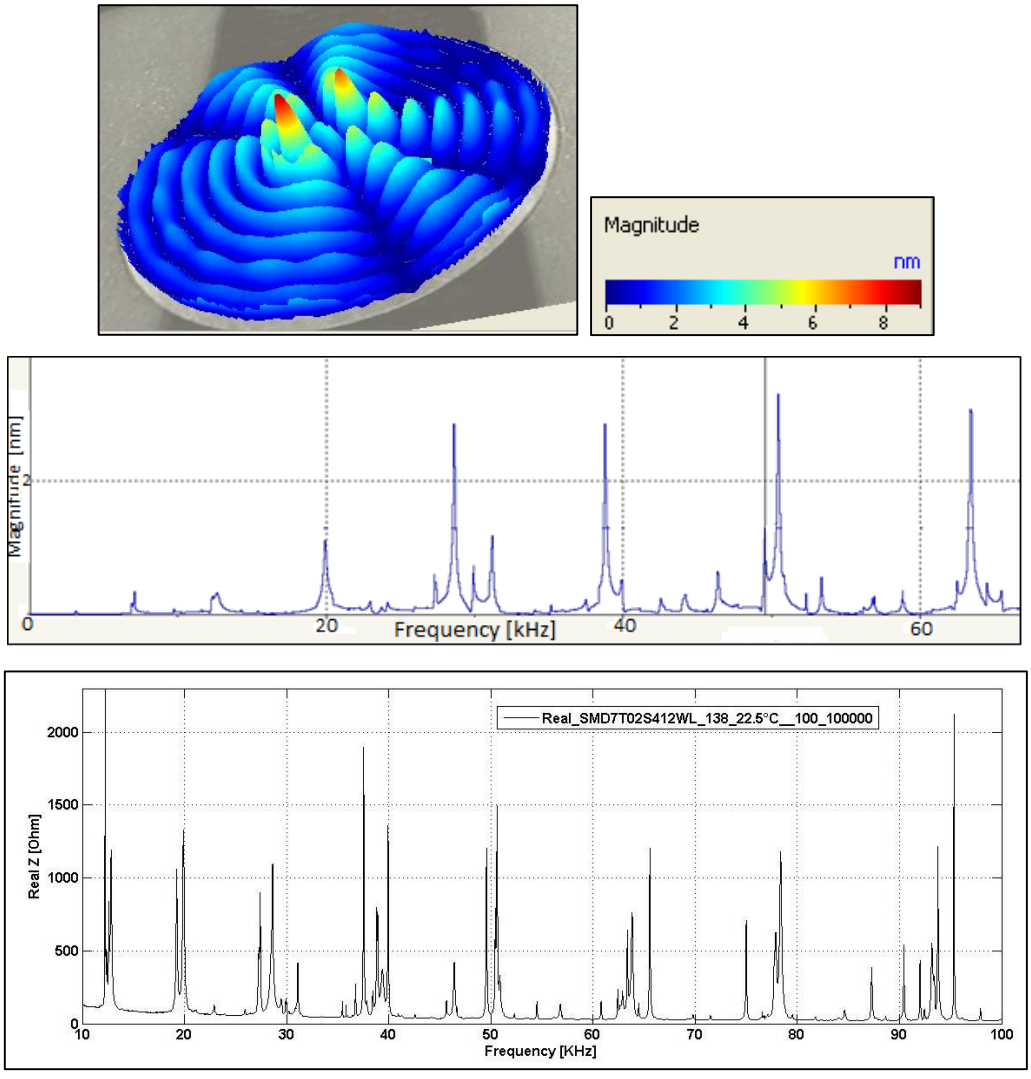

Fig. 6 – Recordings in frequency domain done with SLDV on specimen disk #138 (below is given the EMI signature of the disk)

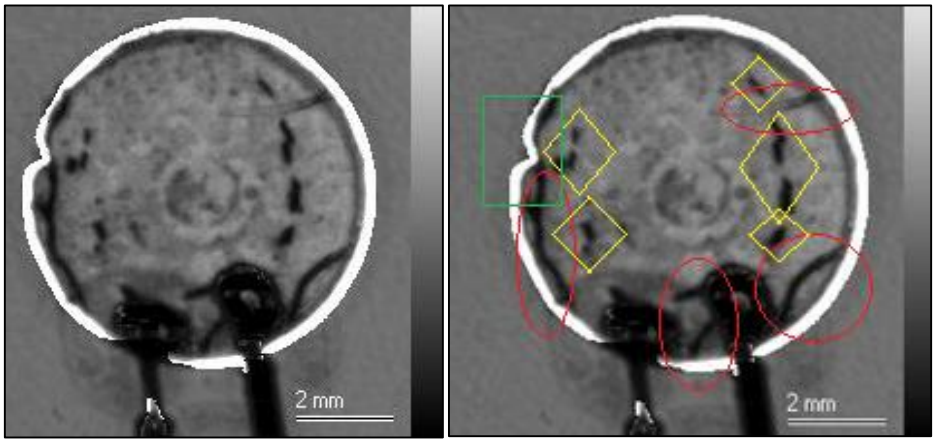

Fig. 7 – Images obtained with SAM 300 scanning acoustic microscope, at investigating the disk #122

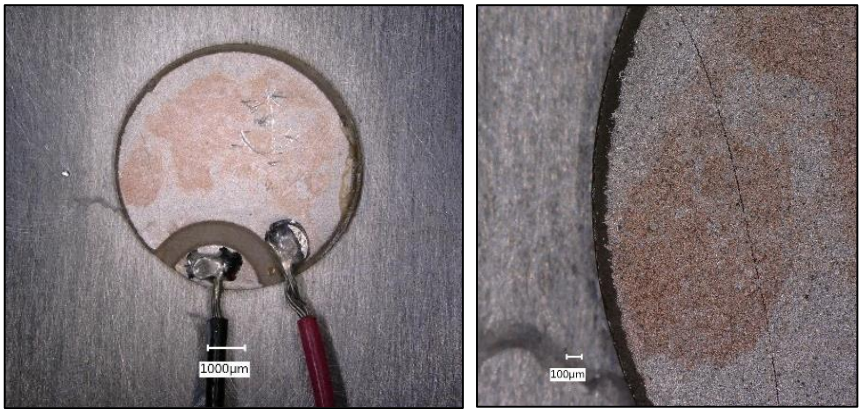

Fig. 8 – Images obtained with digital microscope VHX 5000, disk #106

Concerning first property of NN, lately the literature of domain distinguishes between two concepts: learning and training functions. The training function is the overall algorithm that is used to train NN to recognize a certain input and map it to an output. A common example is backpropagation [15], [19], [20], [21] and its many variations and weight/bias training. A learning function deals with individual weights and thresholds and decides how those would be manipulated. These usually (but not always) employ some form of gradient descent [15], [19].

"Backpropagation" is the abbreviation for "backward propagation of errors", and is a common method of training used in conjunction with an optimization method such as gradient descent.

The method calculates the gradient of a loss function with respects to all the weights in the network. The gradient is fed to the optimization method which in turn uses it to update the weights, in an attempt to minimize the loss function.

Gradient descent is based on the observation that if the multivariable function $f(x)$ is defined and differentiable in a neighborhood of a point a, then $f(x)$ decreases fastest if one goes from a in the direction of the negative gradient $f(x)$ at a, $-\nabla f(a)$.

Consider the problem of approximation of a function given by samples $\left(x_1, y_1; x_2, y_2; ...; x_Q, y_Q\right)$ using a multilayer feed-forward NN. To illustrate the architecture, the mathematical model and the NN operation, we refer to the detailed scheme from Fig. 9. Generally, the number of nodes in the input and output layers can be determined by the dimensionality of the problem. However, determining the number of hidden nodes is not straightforward. It requires first the determination of the number of hidden lavers. There is a number of theoretical results concerning the number of hidden layers in a network. Specifically, in [20] it has shown that a network with two hidden layers can approximate any arbitrary nonlinear function and generate any complex decision region for classification problems.

Thus, a three-layers NN with 5, 10 and 1 "neuron", is defined and trained to approximate the EMI of a monitored structure. Specifically, NN will approximate the real part of the EMI and the training effort will quantify the damage level of the structure. The outputs of the three layers are denoted as

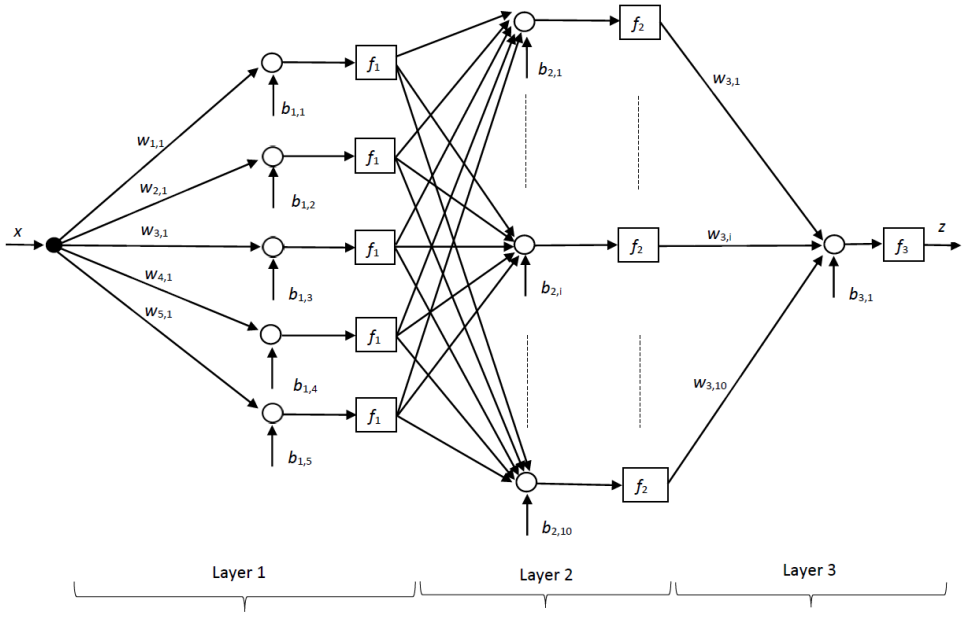

Fig. 9 – Detailed diagram of a three-layer NN

$$a_1 = F_1\left(W_1 x + b_1\right), \quad a_2 = F_2\left(W_2 a_1 + b_2\right), \quad z = W_3 a_2 + b_3 \tag{3}$$

$x \in R$ is the NN input and $z \in R$ is NN output. $W_1 \in R^{n_1 \times 1}$, $W_2 \in R^{n_2 \times 1}$, $W_3 \in R^{1 \times n_2}$ are the weight matrices.

The output of the neuron layers are $a_1 \in R^{n_1 \times 1}$, $a_2 \in R^{n_2 \times 1}$ respectively; n_1, n_2 and n_3 are the numbers of neurons in the input, "hidden" and output layers, respectively. We have noted so-called activation functions $F_1 := \left[f_1, f_2, ..., f_5\right]^{\mathrm{T}}, F_2 := \left[f_1, f_2, ..., f_{10}\right]^{\mathrm{T}}, F_3 := f_3$ with the observation that all components will be considered identical with $f\left(x\right) = \left(1 + \mathrm{e}^{-x}\right)^{-1}$. Further it is described a sketch of the training algorithm based on steepest descent method.

The approximation problem is thus transformed into an optimization problem defining a function as half of the squared approximation error

$$E_k^q\left(W_1,B_1,W_2,B_2,W_3,B_3\right)=\frac{1}{2}\left[y_k\left(q\right)-z_k\left(q\right)\right]^2 \tag{4}$$

$q=1,\ldots,Q,k=1,\ldots,K$ where Q is the number of the input-output pairs in the training process and *K* is the number of the epochs (number of sweeps of the input-output pairs). The gradient descent method involves the weights updating in the opposite direction of the gradient of the function E which is to be minimized

$$W_i^{new}=W_i^{old}-\alpha\frac{\partial}{\partial W_i}E_k^q\left(W_1,B_1,W_2,B_2,W_3,B_3\right),B_i^{new}=B_i^{old}-\alpha\frac{\partial}{\partial B_i}E_k^q\left(W_1,B_1,W_2,B_2,W_3,B_3\right) \tag{5}$$

with $i=1,2,3$ and α a so-called positive learning rate. The backpropagation method will provide recurrent relations for the weights update starting from initial guess (usually, the algorithm selects random numbers)

$$\begin{gathered}S_3=E,\ S_2=\dot{F}_2\left(W_1p+B_1\right)W_3^TS_3,\ S_1=\dot{F}_1\left(W_2A_2+B_2\right)W_2^TS_2\\ W_1^{new}=W_1^{old}+\alpha S_1p,\ W_2^{new}=W_2^{old}+\alpha S_2A_1^T,\ W_3^{new}=W_3^{old}+\alpha A_2^TS_3\\ B_1^{new}=B_1^{old}+\alpha S_1,\qquad B_2^{new}=B_2^{old}+\alpha S_2,\qquad B_3^{new}=B_3^{old}+\alpha S_3\end{gathered} \tag{6}$$

$$\dot{F}_i\left(\ \right):=\begin{bmatrix}\dot{f}_i\left(\ \right) & 0 & \ldots & 0\\ 0 & \dot{f}_i\left(\ \right) & \ldots & 0\\ \ldots & \ldots & \ldots & \ldots\\ 0 & 0 & \ldots & \dot{f}_i\left(\ \right)\end{bmatrix}_{n_i\times n_i} \tag{7}$$

Let's remark the updating in "inverse" sense, from output to input, of the first relationship (6), and then remark the updating in "direct" sense, input-output, the vectors of weights and biases (the last two relations in (6)). As an example of operation of the algorithm for the proposed NN, consider the approximation of the function $y\left(x\right)=\sin\left(2\pi x\right)+2\cos\left(2\pi x\right)$ on the interval. In this interval 402 sampling points, including the interval heads, were considered and now the weights and biases are updated according to the result of (6). Let's move forward, with the second pair, $\left(x_2,y_2\right):=\left(0,2\right).$ Other updating schemes could be applied, for example, the weights to be taken after completing all 402 points. The procedure will be repeated for a convenient number of iterations (epochs) to ensure a suitable error of approximation.

It seems that NN made a good and relatively fast approximation according to the following relationships and Fig. 10

$$E=\frac{1}{2}\sum_{q=1}^{Q}\left[y\left(q\right)-z\left(q\right)\right]^2=0.4336,\ E\left(1\right)=\frac{1}{2}\left[y\left(1\right)-z\left(1\right)\right]^2=0.0526 \tag{8}$$

$$\begin{gathered}W=\left[0.6194\quad 0.6153\quad 0.1226\quad 0.1238\quad 0.2845\quad 0.7357\quad 0.4113\quad 0.829\quad 0.9351\quad 0.3991\right]\\ W=\left[-5.1555\quad 5.4789\quad -3.0089\quad -1.5854\quad -2.0598\quad 3.7773\quad -1.5568\quad 7.0244\quad 5.3997\quad 1.0201\right]\end{gathered} \tag{9}$$

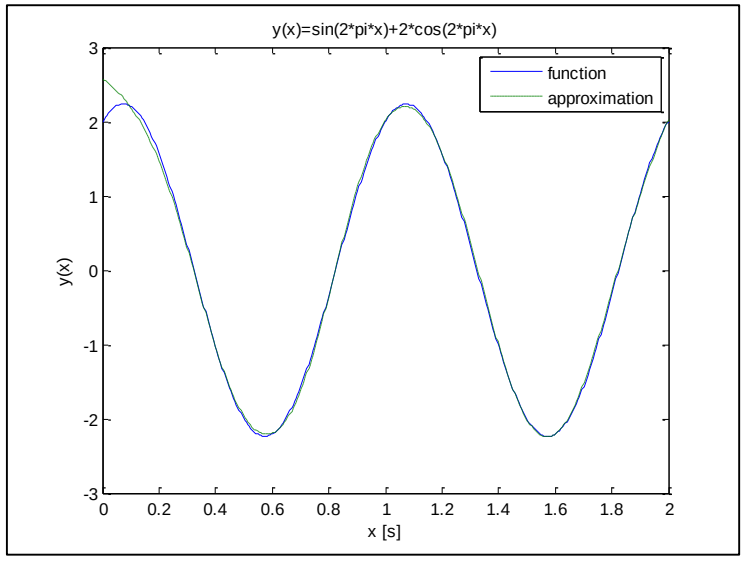

Fig 10 – Working of backpropagation algorithm. Case study

It is well known the peculiar sensitivity of back stepping to the initial choice of weights and biases [19]. Also, the algorithm has a slow convergence, because its step sizes should be adequate to the gradients. The method still remains one of the most significant breakthroughs for training NN. The backpropagation algorithm was greatly improved by the Gauss-Newton algorithm and, further, by the Levenberg-Marquardt (LM) algorithm. The later interpolates between the two algorithms. As the second-order derivatives of the total error function E, Hessian matrix H gives more proper evaluation on the change of gradient vector. As can be seen from the relationship below, the well-matched step sizes are given by the inverted Hessian matrix

$$W^{new} = W^{new} - \alpha g, -g = H\Delta w, W^{new} = W^{old} - H^{-1}g, H := \left[\frac{\partial^2 E}{\partial w_i \partial w_j}\right] \tag{10}$$

In the basic assumption of Gauss-Newton method, the relationship between Hessian H and Jacobian matrix J is

$$H \approx J^T J, J := \left[\frac{\partial E_{ij}}{\partial w_k}\right] \tag{11}$$

In order to make sure that the approximated Hessian matrix in (11) is invertible, the LM algorithm introduces another approximation to Hessian matrix

$$H \approx J^T J + \mu I, \mu > 0, I - \text{the identity matrix} \tag{12}$$

In the following, to apply the proposed online identification scheme, was used the LM algorithm from Matlab, Neural Network Toolbox package. Figs. 11 and 12 show that working of the online identification scheme is made in two steps.

In a first, offline step, based on knowledge and thorough analysis of the structure being monitored, a frequency band is selected, that which is the most sensitive to changes produced by the appearance of damages in the spectrum of EMI recording.

NN learning algorithm will be trained to recognize the healthy form of the EMI spectrum in the specified frequency band. The second step is an online one.

In the case of significant changes occurrence in the spectrum, the algorithm will notify this as a significant error.

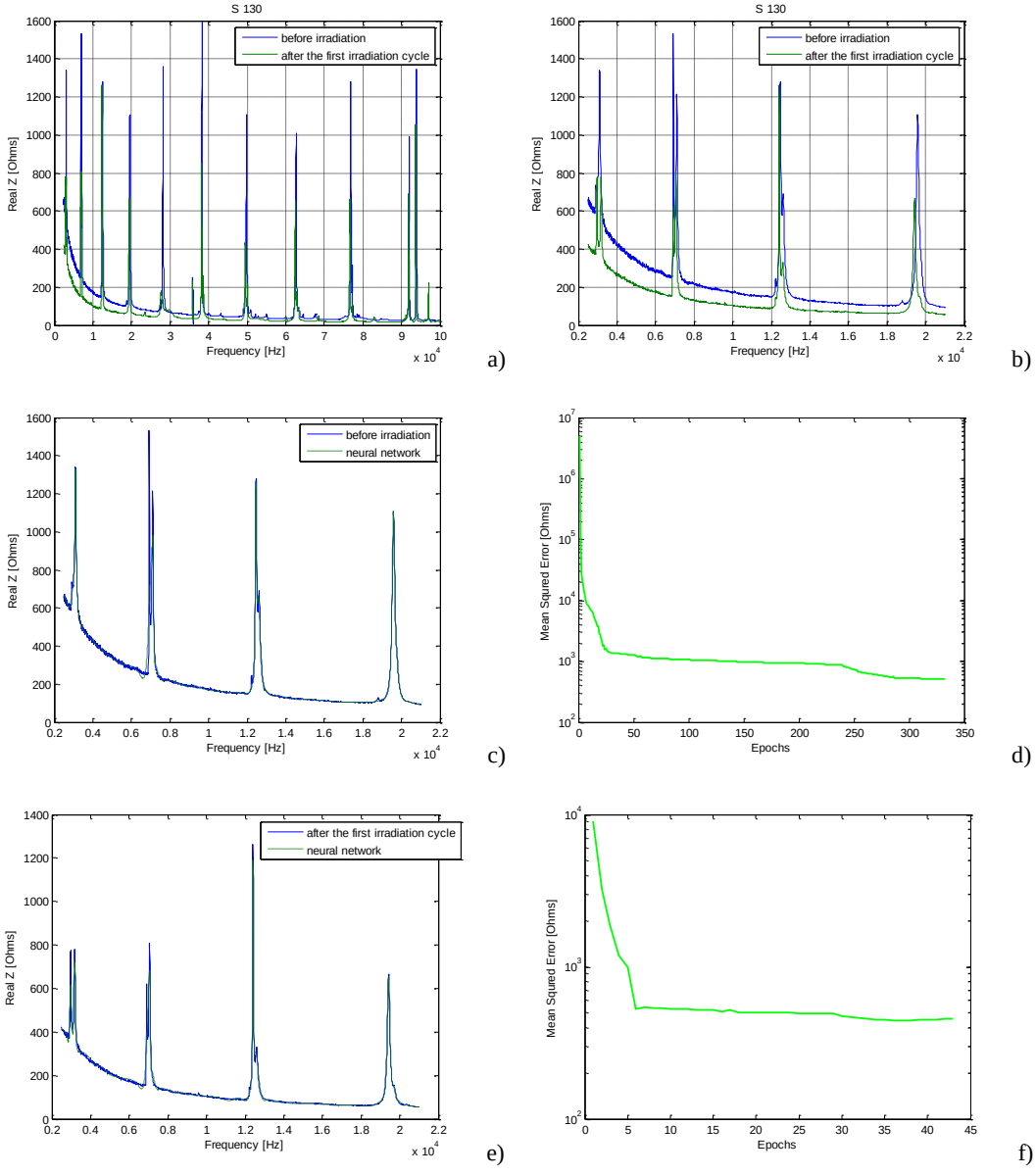

Fig 11 – Online damage identification, over four resonance peaks, based on LM training of NN: a) EMI recording based on tests; b) focus on the first four resonance peaks; c) algorithm training on the window of four resonance peaks representing healthy structure; d) learning validation, use of mean square error criterion; e) online identification of damaged structure; f) damage identification, using mean square error criterion

The notified error is important to be recorded and communicated in real time as a warning to the general SHM system. Then, the NN adapts and learns in principle the new EMI form, assuming that the event is not a catastrophic one.

NN algorithm with healthy EMI characteristic learned is introduced in the online SHM system. In numerical simulations, the proof of damage detection is as follows: after the NN has learned healthy EMI form, insert a form that resulted from tests representing damaged system. At this time, the algorithm is initialized with the last weights corrected representing the healthy system, thus mimicking a real situation.

Algorithm will give at output a quickly increased of the error, which in fact will mark the appearance of the damage.

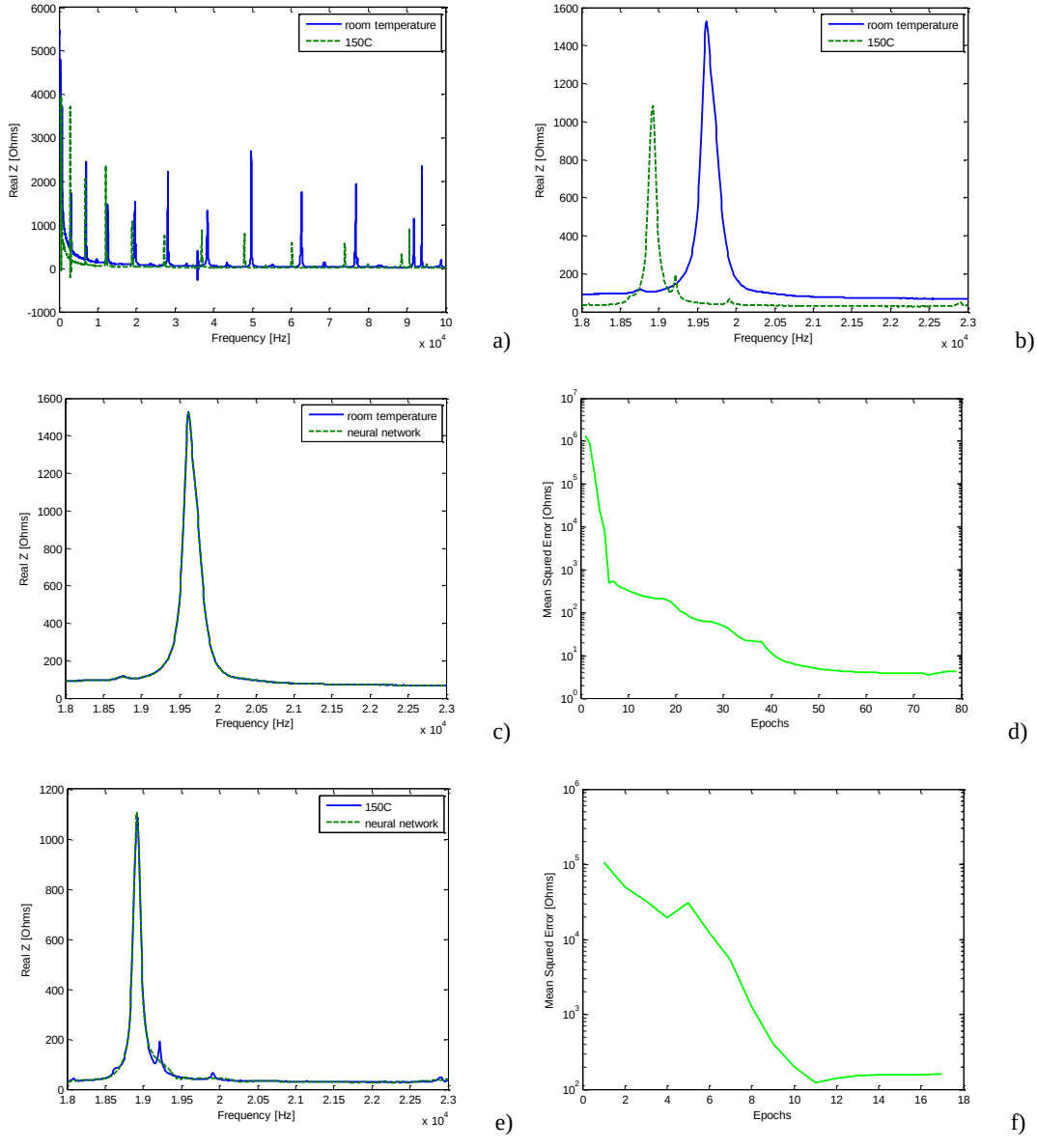

Fig. 12 – Online damage identification, over one resonance peaks, based on LM training of NN: a) EMI recording based on tests; b) focus on the first four resonance peaks; c) algorithm training on the window of four resonance peaks representing healthy structure; d) learning validation, use of mean square error criterion; e) online identification of damaged structure; f) damage identification, using mean square error criterion

4. RESULTS, DISCUSSION AND CONCLUSIONS

One of the major ambitions of modern engineering is to perform SHM in real time in components of high cost and reliability. Thus, the creation or improvement of techniques that enhance the accuracy and reliability of the SHM in Space applications is highly desirable [23].

A preliminary conclusion of the complex tests to validate SHM technology in harsh conditions: EMI signature shows that some specimens were taken out of service, after completing tests in harsh conditions. Careful diagnosis of these faults is in the process of being made, but we can already say that a leading cause for the specimen decommissioning is the lack of a standardized procedure for bonding the sensor on structure. Tables 1-3 constitute an argument for the validity and utility of statistical indicators RMSD and CC in identifying defects offline. Thus, the indicator RMSD varies almost monotonically decreasing with distance from the piezo sensor to defect, what is an intuitive fact. Also, it can be seen that the higher the defect edge makes a larger angle to sensor center, the impact of the increasing deviation from healthy structure, quantified by the indicator RMSD, is higher.

The main result of Section 3 is the proposal of a strategy for online identification of structural damages, using NN in his quality of universal approximator of the nonlinear functions. It is shown that a NN, trained on a LM algorithm, has the willingness to "learn", thus identifying a function more or less complicated, as is the case with the real part of EMI characteristic. Figures 11and 12 illustrate this on a frequency band comprising four peaks or one peak resonance, respectively, for two EMI recordings. NN used to identify the occurrence of the damage in Figs. 11, 12 has three layers: (10, 10, 1) neurons. 1851 or 801 points x_i were considered in the domains of definition of the real parts of some EMI records in the two Figs. Error criterion for training and identification of damage is the mean square error criterion

$$E = \frac{1}{N}\sum_{q=1}^{Q}\left[y(q) - z(q)\right]^2 \tag{13}$$

Here's an example for the weights W_3 obtained at the automatic stopping of the learning process for damage identifying, considering a default value for E

0.0106	-0.9789	-0.0312	0.6531	-0.0630	0.5186	-0.3754	0.5924	1.6549	0.2788
-0.5009	0.2721	0.7401	-0.2801	-0.8083	0.6027	0.9455	-0.9659	-0.0462	0.2830
-0.5341	-0.9522	-0.5465	-0.3506	0.7530	-0.5543	0.6431	0.3854	-0.0864	0.5013
0.2348	0.0115	-0.6683	-0.0763	0.4225	-0.2366	-4.0795	-0.6530	-1.8344	-0.2328
-0.4505	0.6797	-0.7645	0.1253	-0.1322	-1.2936	2.6575	0.6704	-0.3747	0.0993
0.0242	0.4690	-0.8721	-0.5533	-0.0883	-0.5888	3.5430	-0.8349	0.1804	1.5009
0.0259	-0.8812	0.8620	-0.5824	-0.1766	1.1087	2.7861	0.4143	-0.0396	1.1322
0.3425	0.0470	0.0550	-0.6418	0.7408	0.9628	0.4769	0.1718	-0.0780	0.0100
-0.6213	-0.8678	0.5371	-0.9527	-1.0573	1.1338	0.8713	-2.2384	0.9984	0.7846
-0.3600	0.6632	-0.9232	-0.2491	-0.9082	-0.6109	-0.2733	-0.4737	0.3541	0.0224

In view of NN preparation for in-situ installing, at least the following aspects must be elucidated: setting the number of learning iterations; evaluation of common damages that can appear in the structure; investigations on their evolution time; investigations on the possible values of learning errors; the default value of error to stop the learning process.

The Larson-Miller parameter is a means of predicting the lifetime of material vs. time and temperature using a correlative approach based on the Arrhenius rate equation. The value of the parameter is usually expressed as $L=T(C + \log t)$ where C is a material specific constant often approximated as 20, t is the time in hours and T is the temperature in Kelvin. The Larson-Miller parameter describes the equivalence of time at temperature for steel under the thermally

activated creep process of stress rupture. It permits the calculation of the equivalent times necessary for stress rupture to occur at different temperatures. It has the general form

$$L = 0.001T\left(20 + \log t\right) \tag{14}$$

L is the Larson-Miller parameter; T is the temperature in degrees Rankine (°F + 460); t is the time in hours for an isothermal condition.

ACKNOWLEDGEMENTS

The authors gratefully acknowledge the financial support of the National Authority for Scientific Research−ANCS, UEFISCSU, through STAR research project code ID 188/2012.

Special thanks are addressed to Prof. V. Giurgiutiu for the support in making measurements and recordings to LAMSS–USC.

The authors also thank their colleague Eng. Mihai Tudose for important contributions in the achievement of the project.

REFERENCES

[1] D. M. Peairs, B. Grisso, D. J. Inman, K. R. Page, R. Athman, and R. N. Margasahayam, Proof-of concept application of impedance-based health monitoring on space shuttle ground structures, *NASA-TM-2003-211193*, October 2003.

[2] B. Lin, V. Giurgiutiu, P. Pollock, B. Xu, and J. Doane, Durability and survivability of piezoelectric wafer active sensors on metallic structure, *AIAA Journal*, ISSN: 0001-1452, vol. **48**, no. 3, pp. 635-643, 2010.

[3] G. Santoni-Bottai and V. Giurgiutiu, Damage Detection at Cryogenic Temperatures in Composites using Piezoelectric Wafer Active Sensors, *Structural Health Monitoring – an International Journal*, ISSN: 1475-9217, vol. **11**, online first June 28, 2012.

[4] I. Ursu, V. Giurgiutiu, and A. Toader, Towards spacecraft applications of structural health monitoring, *INCAS Bulletin*, (P) ISSN 2066–8201, (E) ISSN 2247–4528, vol. **4**, no. 4, DOI: 10.13111/2066-8201.2012.4.4.9, pp. 111-124, 2012.

[5] A. J. McDonald, and J. R. Hansen, Truths, Lies, and O-rings – Inside the Space Shuttle Challenger disaster, *University Press of Florida*, Gainsville, FL, 2009

[6] * * * http://www.nasa.gov/columbia/home/CAIB_Vol1.html, *NASA, Report of Columbia Accident Investigation Board*, vol. **1**, August 2003.

[7] S. Mancini, G. Tumino, and P. Gaudenzi, Structural health monitoring for future space vehicles, *Journal of Intelligent Material Systems and Structures*, ISSN: 1530-8138, vol. **17**, pp. 577-585, 2006.

[8] D. Enciu, M. Tudose, B. Neculaescu, A. Toader, I. Ursu, Damage identification and damage metrics in SHM (structural health monitoring), AEROSPATIAL 2014, 18-19 september 2014, Bucharest, Romania, *Proc. of AEROSPATIAL 2014*, to be published, ISSN: 2067-8614.

[9] C. Rugina, A. Toader, V. Giurgiutiu, I. Ursu, The electromechanical impedance method for structural health monitoring of thin circular plates, *Proceedings of the Romanian Academy, Series A, Mathematics, Physics, Technical Sciences, Information Sciences*, 2014, ISSN : 1454-9069, vol. **15**, no. 3, pp. 272–282

[10] C. Rugina, V. Giurgiutiu, A. Toader, I. Ursu, The electromechanical impedance method on thin plates (see *http://www.imsar.ro/Sisom_2014.pdf*).

[11] T. Li, F. Jiang, E. A. Olevsky, K. S. Vecchio, M. A. Meyers, Damage evolution in Ti6Al4V–Al3Ti metal-intermetallic laminate composites, *Materials Science and Engineering, A*, ISSN: 0921-5093, **443**, pp. 1–15, 2007.

[12] * * * *Instruction Bulletin B-130* (Vishay Precision Group; Instruction Bulletin B-129-8; M-Bond 610).

[13] V. Giurgiutiu, *Structural Health Monitoring with Piezoelectric Wafer Active Sensors*, Elsevier Academic Press, ISBN 978-0120887606, 2008.

[14] I. Ursu, Daniela Enciu, A. Toader, Towards structural health monitoring of Space vehicles, to be submited.

[15] R. Rojas, *Neural networks. A systematic introduction*. Springer Verlag, Berlin, ISBN: 3540605053, 1996.

[16] I. Ursu, F. Ursu, *Active and semi-active control*, Romanian Academy Publishing House (in Romanian), ISBN: 973-27-0894-8-1, 2002.

[17] G. Cybenko, Approximations by superposition of sigmoidal functions, *Mathematics of Control, Signals, and Systems*, ISSN: 0932-4194, **2**, no. 4, 303-314, 1989.
[18] A. N. Kolgomorov, On the representation of continuous functions of several variables by the superposition of continuous functions of one variable and addition. Doklady Akademiia Nauk SSR, **114,** pp. 953–6, 1957.
[19] C. M. Bishop, *Neural networks for pattern recognition*, Clarendon Press, Oxford, ISBN: 9780198538646, 1995.
[20] D. E. Rumelhart, G. E. Hinton, R. J. Williams, Learning representations by back-propagating errors, *Nature* ISSN: 0028-0836, **323**, pp. 533 – 536, 1986.
[21] R. Hetcht-Nielsen, Theory of the backpropagation neural networks, *Proc. Inter. Joint Conf Neural Networks*, ISSN: 0018-9219, vol. **I**, June 1989, pp. 593-61 1, 1989.
[22] * * * http://www.nasa.gov/pdf/379068main_Temperature_of_Space.pdf
[23] V. Giurgiutiu, I. Ursu, A. Toader, M. Arghir, C. Postolache, C. Rugina, D.-D. Prunariu, Sensors and Methods for Structural Health Monitoring of Space Vehicles, Chapter in the book *Advances in structural health monitoring of space systems*, Editor Andrei Zagrai, New Mexico Institute of Technology, Co-editors: Brandon Arritt and Derek Doyle, Air Force Research Laboratory, Space Vehicles Directorate, Publisher: Wiley & Sons, to be published in 2015.